J Nondestruct Eval (2011) 30:237–245
DOI 10.1007/s10921-011-0112-x

Enhancing Probability of Detection and Analysis of Bolt Hole Eddy Current

P.R. Underhill · T.W. Krause

Received: 16 December 2010 / Accepted: 7 July 2011 / Published online: 28 July 2011

Abstract Fatigue cracks are prone to develop around fasteners found in multi-layer aluminum structures on ageing aircraft such as the CC-130 Hercules and CP-140 Aurora (P-3 Orion). Probability of Detection (POD) studies using eddy current techniques within the bolt holes contribute to risk assessments used in evaluating the serviceability of these aircraft. Improving POD by optimizing the inspection system can reduce the required frequency of inspections, since assurance of detection of smaller crack sizes extends the interval for which growth of cracks to a critical size may occur. In this work signal analysis and POD of laboratory grown fatigue cracks in the corners of bolt holes of 7075-T6 aluminum is examined. A number of parameters that enhance crack detection are identified, including the use of intimate contact probes versus steel sheath (non-contact), higher frequencies and the use of C-Scan display. Results demonstrate better detectability at 1600 kHz, than at the normally used 400 kHz, and enhanced recognition and assurance of identification of peak crack signal for data recorded and displayed in a C-Scan format. Results are compared with a previous POD study, which used current field techniques for detection.

Keywords Eddy current · Aluminum · POD · Aluminum 7075-T6 · Cracks

1 Introduction

Eddy current testing is widely used as a Nondestructive Testing (NDT) method for first detecting cracks and second determining their size in metallic structures. In particular, the technique is widely used in the aircraft industry to check for cracks in bolt holes. An important parameter describing such methods is the Probability of Detection (POD), which specifies the probability of detecting a crack of a certain minimum size, a certain fraction of the time [1]. Fatigue cracks in multi-layer aluminum structures are prone to develop around the fasteners found on ageing military aircraft such as the CC-130 Hercules and CP-140 Aurora (P-3 Orion). Sufficient POD of fatigue cracks in the bolt holes of 7075-T6 aluminum structures using eddy current techniques is critical for the continued service of these aircraft. POD information is used in risk assessments, drives scheduled maintenance and determines inspection intervals for damage tolerance, i.e. the detection of a crack before it can grow to a critical size. The smaller the crack that can be reliably detected, the longer the inspection intervals can be. Enhancing POD can therefore, result in significant economic benefits by reducing the frequency of inspections.

Recently a large POD study of cracks located at the corner of 4.6 mm (0.182 inch) diameter holes in Al 7075-T6 was conducted [2] within the Canadian Forces (CF). The study involved over 468 coupons including 45 electro-discharge machined (EDM) corner notches, 72 fatigue corner cracks and 351 blank specimens. The investigation involved 24 qualified operators at different sites and maintenance centres across the country. The equipment used was a Stavely Nortec 2000D eddy current instrument and a Stavely RA 2000 rotating bolt hole scanner with a split-D differential coil. The diameter of the stainless steel (non-contact) probe itself was 4.29 mm (0.169 inch) providing a maximum clearance of 0.38 mm (0.015 inch) between the hole and the probe. Measurements were conducted at 400 kHz with detection dependent on real-time identification of a discontinuity signal in the instrument's impedance plane display,

P.R. Underhill · T.W. Krause (✉)
Dept. of Physics, Royal Military College of Canada, Kingston, Ontario, Canada
e-mail: Thomas.Krause@rmc.ca

as scans were not normally recorded. The results showed substantial scatter and only produced an $a_{90/95}$ of 0.91 mm for the fatigue cracks and 0.79 mm for the EDM notches. $a_{90/95}$ is widely used as the measure of detectability for aerospace applications and is the crack size for which at least 90% of the cracks can be detected, established with 95% confidence. The methods used for determining POD are described in MIL Handbook 1823 (2007 Update) [3] and are implemented in a package available on the web [4]. Analysis of the results indicated that a large component of the scatter was due to an inadequate calibration process [5, 6]. When the data was reanalyzed with an attempt to compensate for this calibration issue the $a_{90/95}$ was reduced by 10 to 20%. This still resulted in an unacceptably large value of $a_{90/95}$ for the intended application. This present study was undertaken to understand the parameters affecting POD and to look at the use of C-scan and alternate frequencies to improve the detectability of corner cracks.

2 Experimental

For the first two parts of this study, eddy current data was obtained from three sets of specimens using an Olympus MS5800 eddy current instrument equipped with an RA2000 rotating bolt hole scanner. Two probes were used to collect the data. The first was a 4.62 mm (0.180 inch) diameter intimate contact probe equipped with a split-D sensor used to collect the data in differential mode. The split-D probe is mounted on one of two plastic backings that are splayed in order for the surface probe to remain in contact with the hole walls. The second was a stainless steel (non-contact) probe of the same diameter, also with a split D sensor. Data was collected at four frequencies 200, 400, 800 and 1600 kHz. The lift off component was determined by placing the rotating probe against the surface of the specimen. It was rotated to the horizontal direction and the data was presented initially as a C-scan of the vertical component. The gain of the system at each frequency was initially set using a 0.30 mm (0.076 inch) EDM corner notch so that it gave a signal length of one volt. The gain was then kept fixed, maintaining system response, throughout the rest of this study. Signal length (volts peak to peak) was chosen for calibration because it and phase angle, are independent of each other, while signal height is a composite of the other two (height = length*sin (phase angle)) as shown in Fig. 1. To take the C-scan, the RA2000 head was mounted on a motorized stage and driven through the hole at constant speed. The C-scan data could be further visualized as the vertical component versus time and sections of the data could be viewed as a Lissajou figure. The data was collected at a rotational speed of 1500 rpm largely because this is the speed used in a recent Department of National Defence POD study organized by the National Research Council of Canada [2].

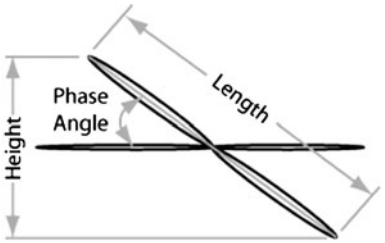

Fig. 1 Idealized Lissajou figure from a single rotation of the probe illustrating the length (in Volts peak to peak, V_{pp}), height (V_{pp}) and phase angle measurements

The first set of specimens consisted of corner fatigue cracks that were grown in 9.5 mm (3/8 inch) thick 7075-T6 plates using EDM starter notches. An undersized hole was drilled through the specimen and an EDM starter notch was created. Once the cracks had been grown to the desired size, the holes were drilled out to 4.62 mm (0.182 inches), eliminating the starter notch. The dimensions of the cracks were measured by fastening the specimens in a load frame and placing them under tension. Silicone replicas (Repliset) of the inside of the hole and the front face were made and the size of the cracks were determined from these. Crack length is the dimension along the bore of the hole and crack depth is the dimension perpendicular to the bore of the hole as defined elsewhere [5, 6]. This specimen set was part of a large investigation that has been reported in several places in the literature [5–7]. The primary issue with this data set was that the smallest fatigue cracks had very unrealistic aspect ratios. In most normal applications the aspect ratio of a corner crack (depth:length) is approximately 1:1. Some of the smaller cracks in this set had aspect ratios up to 1:17. The average aspect ratio at larger sizes was 1:1.7 [6, 7]. Also, for many of the specimens with large cracks, it became clear through C-scan images that there were, in fact, multiple cracks present.

A second set of specimens were created by drilling a 4.62 mm hole through 3.06 mm (1/8 inch) 7075-T6 rolled sheet. The holes were in the center of 25.4 mm wide by 152 mm long (1 × 6 inch) specimens. The front and back faces were sanded with either 300 or 600 grit emery paper to eliminate any burrs at the edges of the hole. The specimens were then placed in a hydraulic load frame and cycled in tension and compression ($R = -0.67$) at a maximum load of 12 kN (approximately 520 MPa, assuming a K_t of 3) for 8000 cycles. The specimens were then loaded to 8 kN and examined using a hand held RA2000 rotating bolt hole scanner and probe as described above, and a Nortec 2000 eddy current system. The Nortec was set up to display Lissajou figures with signals rotated to place the lift-off component on the horizontal axis. The X gain was set to 60 dB and the Y gain to 80 dB. The system was operated at 1600 kHz. If a crack was detected, the specimen was removed from the

load frame and a C-scan was generated by scanning with the MS5800 and motorized stage described earlier. If no crack was detected the specimen was cycled for a further 1000 cycles and then re-examined. The process was continued until a crack was detected. Using the Nortec 2000 system, two false calls were made. No false calls were made using the MS5800 in C-scan mode. Once a specimen was deemed to be cracked, it was broken in the hydraulic load frame to expose the cracks. Crack lengths and depths were measured using an optical microscope.

Finally, a third set of specimens were made using 3/8" thick specimens of 7075-T6 aluminum. These specimens were laid out in the same manner as the specimens in the previous paragraph except that they varied in length. These specimens were also placed in the hydraulic load frame and cycled as before (at three times the load). When the load frame paused, a modified form of the motorized system used earlier automatically collected a C-scan. The specimen was cycled and scanned until it was cracked from face to face. This process provided a sequence of eddy current measurements from the growing cracks.

To determine the size of the eddy current signal, the collected signals were displayed as vertical component versus time and the region of the largest deflection was found. The Lissajou figure from a single rotation corresponding to this region was displayed and measured as shown in Fig. 1.

3 Results

A plot of the measured signal length (V_{pp}) at 200, 400 and 800 kHz versus that at 1600 kHz from a number of cracks from the first sample set is shown in Fig. 2. It can be seen that there is excellent correlation between the measured peak-to-peak lengths at different frequencies. The slopes of the best fit line through each of the 400 and 800 kHz data is 0.95 and that for the 200 kHz data is 0.91, which is not statistically different. The data show that the length of the peak-to-peak signal is almost independent of driving frequency from 200 kHz to 1600 kHz.

A plot of the relationship between the phase angles at different frequencies is given in Fig. 3. Few phase angles below 10° are given because it is difficult to distinguish the signal from the noise due to lift off. It can be clearly seen that phase angle is a strong function of excitation frequency. For the 1600 kHz signal the lowest phase angle recorded for the smallest crack was 20 degrees. In addition, the Lissajou figures associated with cracks tended to be less well formed at lower frequencies. This is attributed to the increased relative affect of noise at these amplitudes, which produces more scatter in the measurement of the phase angles. In most cases, detectability of the signal from a small crack is a function of signal height. From Fig. 1, it is clear

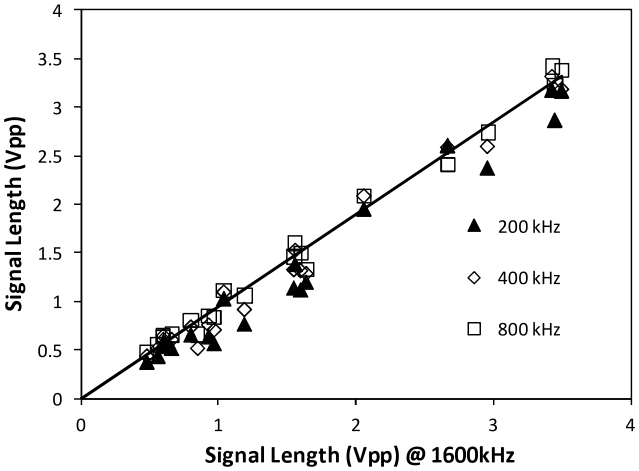

Fig. 2 Plot of signal length at different frequencies versus the length at 1600 kHz for a number of cracks from the first data set. The trend line is for the 400 kHz data

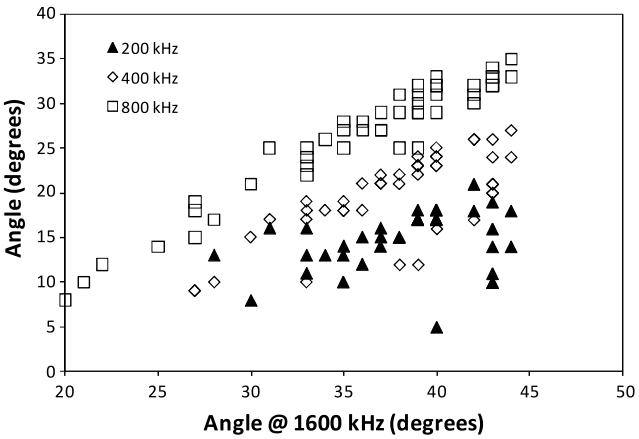

Fig. 3 Phase angle at different frequencies versus phase angle at 1600 kHz for a number of cracks from the third data set

that height is approximately equal to length•sin (phase angle). Hence a signal at 200 kHz will have a much smaller height than the equivalent signal obtained with a 1600 kHz driving signal even though the length of the two signals is nearly the same. Hence the choice of driving frequency will have a strong impact on POD, with the higher frequency signal having a much better POD.

In Fig. 4, the evolution of phase angle as a function of signal height is shown for several cracks taken from the third data set, which continued crack growth until fracture. While there is some crack-to-crack variation, it is clear that the phase angle increases rapidly with height (and crack size) and quickly comes to a saturation level. For a driving frequency of 1600 kHz that limit is approximately 40 degrees. The rapid increase in the phase angle is fortuitous because an increased phase angle improves detectability. One of the factors influencing the phase angle is the ratio of crack depth to skin depth [8]. As the crack depth increases the phase

angle increases. However, once the crack depth is substantially greater than the skin depth, the phase angle ceases to increase.

Figure 5 shows the eddy current signal height obtained at the four driving frequencies used to monitor the crack as it grew to such a size that the signal began to saturate. Saturation occurs because the crack exceeds the size of the detector. This is illustrated schematically in Fig. 6. At the edge of detectability, the crack depth is comparable to the skin depth. As the crack grows, crack depth rapidly exceeds three times the skin depth and the detector becomes completely insensitive to crack depth and only reflects changes in crack length (dimension along the bore hole). At a certain point the crack length exceeds the dimensions of the probe and its associated induced field (approximately 1.8 mm) and the probe is therefore no longer very responsive to further increases in crack size. At this point the signal saturates as shown in Fig. 5. Note that all 4 frequencies saturate at the same time. A plot of signal height versus the signal height at 1600 kHz gives 3 straight lines with decreasing slope as the frequency is lowered.

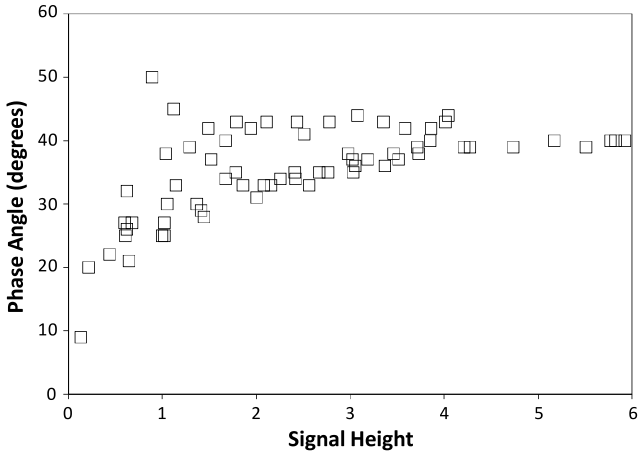

Fig. 4 Phase angle as a function of signal height (vertical V_{pp}) at an excitation frequency of 1600 kHz for a number of cracks from the third data set

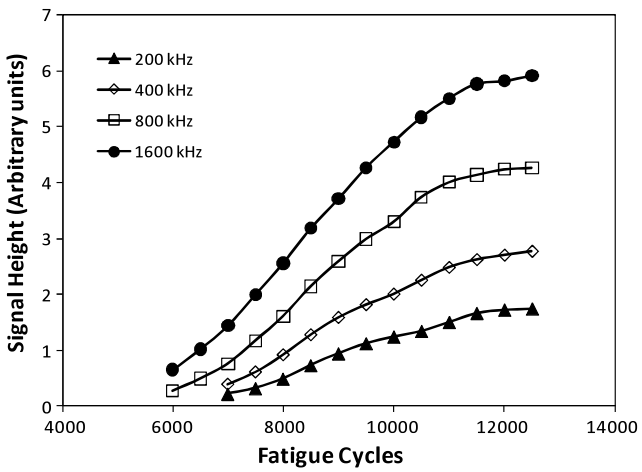

Fig. 5 Signal height versus fatigue cycle from the evolution of a crack in the third data set

While it is true that the 200 kHz signal has a greater depth of penetration (skin depth) in aluminum (0.26 mm @ 200 kHz vs. 0.09 mm@ 1600 kHz), the signal strength is dominated by crack length because the crack length-to-depth ratio for corner cracks is typically 1:1. Hence, in aluminum, even at very small crack lengths, the crack is deeper than the skin depth and hence is no longer sensitive to changes in that dimension as discussed above. In fact, a POD analysis of the data from the corner cracks of the second data set (as outlined below), using a frequency of 1600 kHz, puts $a_{90/95}$ at approximately 0.22 mm for the crack length, which is approximately two and a half times the skin depth.

Continued growth of the cracks as studied for the fatigue crack growth cycle shown in Fig. 5 combined with quantitative fractography can be used to compile data towards a calibration curve. Rather than stopping the experiment at the earliest detection, the crack can be allowed to grow to a substantial size with periodic inspections. The signal magnitude can then be plotted versus crack length as determined by fractography as shown in Fig. 7.

Figure 8 shows a 1600 kHz C-scan image obtained from a small corner crack of length 0.18 mm and the Lissajou figure corresponding to the strongest signal. This small corner crack illustrates the effectiveness of C-scan compared

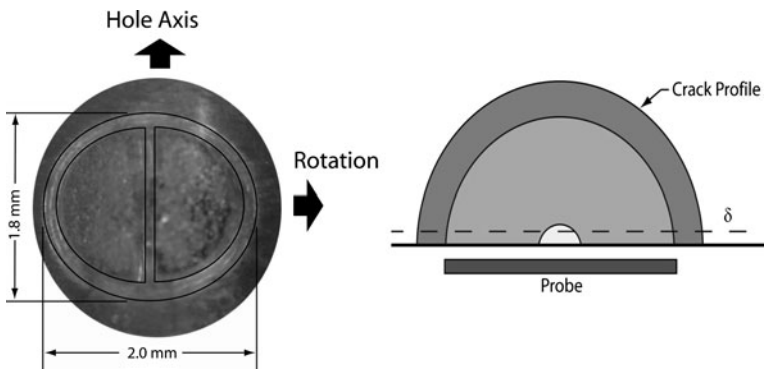

Fig. 6 (*Left*) Magnified view of the split D probe showing its dimensions and orientation. The *black lines* help to demark the coils. (*Right*) Schematic view of crack size relative to the probe dimensions along the *hole axis*

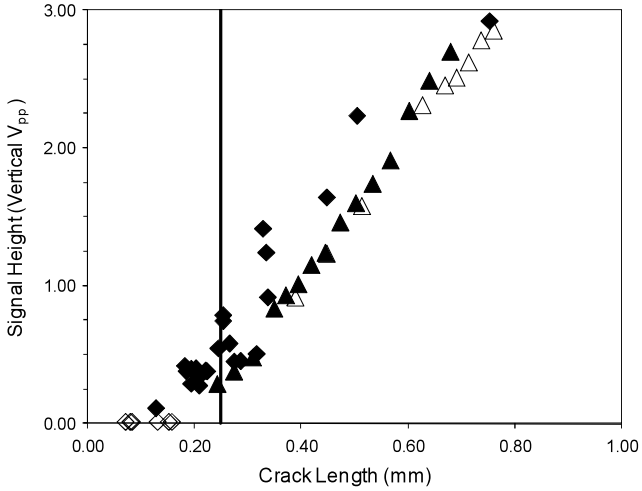

Fig. 7 Signal height versus crack length for corner cracks. The *diamonds* (◆) are from individual specimens with one eddy current measurement per specimen (data set #2). The *open diamonds* (◇) are from undetected corner cracks (data set #2). The *triangles* (△ and ▲) are from two specimens with multiple measurements and crack lengths determined by quantitative fractography (data set #3). The *vertical line* is the $a_{90/95}$ limit for corner cracks using C-scan images for crack detection

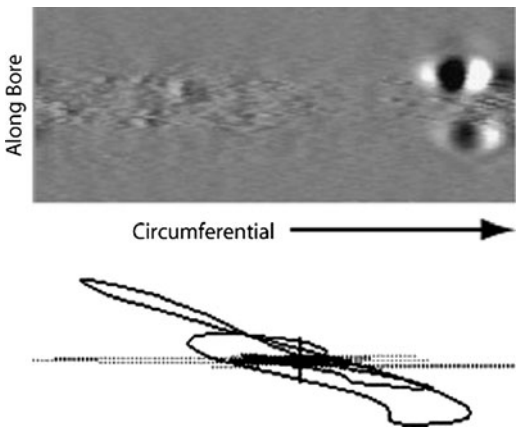

Fig. 8 C-scan (@ 1600 kHz) of a hole with two corner cracks (*top*). The lower crack measured 0.20 mm × 0.18 mm (depth × length). The Lissajou figure (*bottom*) is from the lower crack

with conventional manual eddy current techniques to detect small cracks. The signal from this crack would be difficult to pull out of the noise in a Lissajou figure, especially if the probe were being manipulated by hand. However, because the signals from the C-scan have a characteristic pattern, it is much easier to detect them at small sizes. While the magnitude of the intensity variation depends on crack size, the shape, itself, is only a function of the probe geometry, at least for small cracks near the detection threshold. Because the flaw has a coherent shape, it can be relatively easily detected against the random fluctuations of the background. Image analysis techniques can also improve the estimation of the signal magnitude as they can use information from the

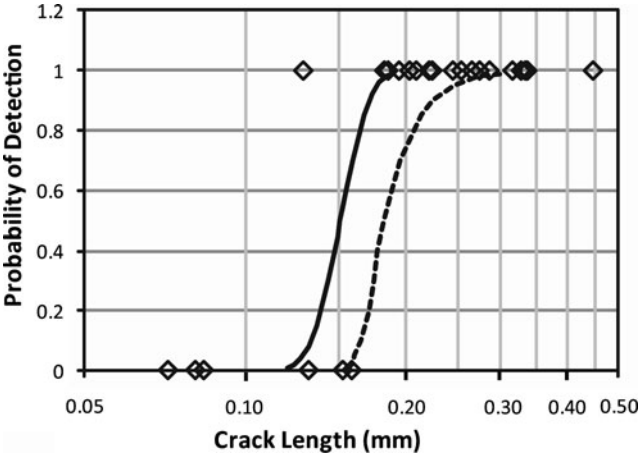

Fig. 9 POD analysis at 1600 kHz of corner cracks from second data set using the proximity probe. The *solid line* is the best fit probit analysis. The *dashed curve* is the 95% upper bound on the probit analysis. The X axis is a log scale

whole shape rather than just the signal height determined from a single line in the image, which is effectively what manual techniques based on the Lissajou figure do. A drawback in the C-Scan display is that only one component, the vertical voltage height, is represented whereas the Lissajou figure displays phase separation and allows immediate identification of the quadrant in which the signal occurs. Work is underway to address this deficiency in the C-scan.

In order to illustrate the capabilities of the C-scan approach a POD analysis of the corner crack data was carried out using a probit function [9]. The analysis was carried out on a hit/miss basis based on the signal from the crack being clearly visible to the eye of the operator in the C-scan image. For this work, the C-scan data was scaled so that the full greyscale range (0–255) corresponded to ±0.20 V. The actual scale did not play much of a role in the detectability of a crack. Setting the greyscale range to ±0.50 V had no effect on the detectability of the cracks. The critical issue for detectability was the coherence of the pattern and whether or not it could be distinguished from the random fluctuations in the image. The actual criterion for identifying a crack was, therefore, somewhat subjective and is reflected in the overlap of the hit/miss data in Figs. 9, 10 and 11. The same scaling was used for the 1600 and 800 kHz data, but as mentioned above the actual scaling had no effect on the detectability of the signals. There were 30 data points available from the second data set. The results of the analysis are shown in Fig. 9 for the proximity probe. The $a_{90/95}$ value is 0.22 mm (0.009 in) using the proximity probe. Six cracks were undetected. The same specimens were also analyzed using the non-contact differential probe of nominally the same diameter. The results of the probit analysis for this data are shown in Fig. 10. The $a_{90/95}$ value at 1600 kHz is 0.29 mm (0.013 in). Table 1 summarizes a_{50}, the mean

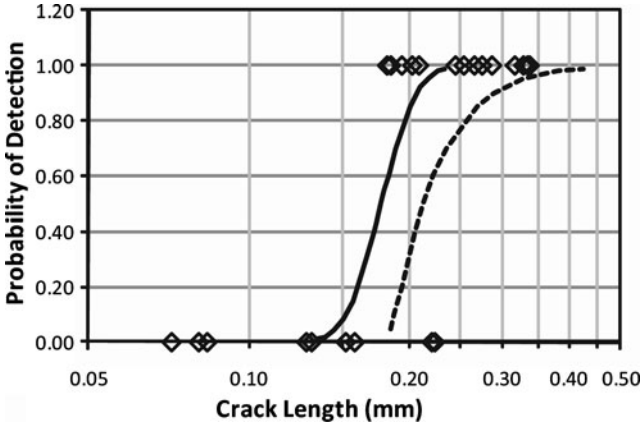

Fig. 10 POD analysis at 1600 kHz of corner cracks from the second data set using the stainless steel (non-contact) probe. The *solid line* is the best fit probit analysis. The *dashed curve* is the 95% upper bound on the probit analysis. The X axis is a log scale

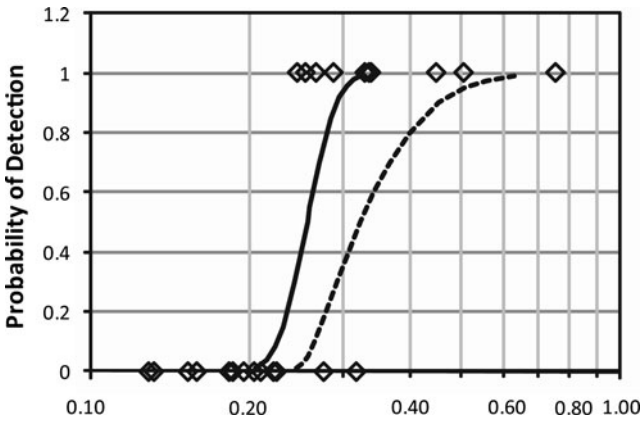

Fig. 11 POD analysis at 800 kHz of corner cracks from the second data set using the proximity probe. The *solid line* is the best fit probit analysis. The *dashed curve* is the 95% upper bound on the probit analysis. The X axis is a log scale

size detected, and $a_{90/95}$ for these cases. The $a_{90/95}$ value of 0.22 mm for the proximity probe was made without any false calls. In part, this was a function of the way the tests were conducted and in part, it illustrates the robustness of using C-scan to identify a crack as will be discussed later. It is the result of setting a high threshold for detectability for this particular technique.

Figure 11 shows the results obtained with the proximity probe operated at 800 kHz. 18 indications were undetected. In this case the $a_{90/95}$ has increased to 0.45 mm, approximately twice the value obtained at 1600 kHz. Table 1 summarizes a_{50} and $a_{90/95}$ values obtained for these cases. The stainless non-contact probe operated at 800 kHz also exhibited a reduced capability to detect cracks with only eight hits obtained. As the number of samples was statistically not sufficient the $a_{90/95}$ value was not calculated. Unfortunately, there were insufficient hits from this data set with cracks long enough to perform an analysis at 400 kHz, as only 4 of the 30 cracks were detected at this frequency. At 200 kHz no cracks were detected.

Table 1 Summary of results for POD of corner cracks from two probe types

Parameter	Freq. kHz	Intimate contact probe	Non-contact probe
a_{50} (mm)	1600	0.15	0.18
$a_{90/95}$ (mm)	1600	0.22	0.29
a_{50} (mm)	800	0.26	0.31
$a_{90/95}$ (mm)	800	0.45	–

4 Discussion

Improvement of POD involves a number of factors. The introduction of new methods and technologies is only one element. Human factors, the inspection environment and sources of noise that arise within in-service bolt holes must be included for a more thorough and realistic POD study. For example, human factors were part of a previous study of bolt hole POD incorporating 24 inspectors [5]. However, the technology associated with methods of data acquisition and display can be used to determine lower limits for detection and improve methods for enhanced detectability, as performed here. Furthermore, currently available technologies allow recording and storage of data in portable units for either later review or as an immediate record of indicators in cases where these are detected.

This work has identified a number of factors leading to the potential improvement of POD in field studies. State-of-the-art technology, which allows data storage, the generation of C-Scans using an encoded semi-automatic scanner and acquisition at multiple frequencies, including higher frequencies than what data is nominally acquired at. Furthermore, the study has been performed on fatigue cracks, without starter notches, providing a closer simulation of cracks that form in-situ. Examination of these cracks has been conducted using fractography, providing more accurate sizing estimates than conventional replica sizing techniques.

The lower $a_{90/95}$ for intimate contact probes when compared to non-contact probes is attributed to both reduced lift-off and limitation of lift-off variation that arises for uncentered steel sheathed non-contact probes. The stainless steel sheathed probes are characterized by good wear characteristics, a feature potentially requiring improvement for intimate contact probes.

The introduction of higher frequencies substantially improves POD relative to that of the lower frequency of 400 kHz normally used for data acquisition. This is shown

in Fig. 5, with the highest frequencies demonstrating higher amplitude response to crack growth earlier in the set of fatigue cycles than lower frequencies. The POD reproduces this result in a comparison of signals at 1600 kHz and 800 kHz where, for example, $a_{90/95}$ changes from 0.22 to 0.45, respectively, for contact probes as summarized in Table 1. These observations can be understood in terms of the voltage signal response dependence on frequency as well as the general skin depth relation. The sinusoidal time-harmonic excitation of the transmit coil produces a variation of flux due to the coil that varies as [8]

$$\Phi = \Phi_0 \cos(\omega t), \tag{1}$$

where ω is the radial excitation frequency and Φ_0 is the peak flux. In the proximity of a conducting material the induced voltage response, which is the combined response of the material and the differential receive coils, is a function of the time derivative of the rate-of-change of flux within the system. For the secondary receive coils with N turns the voltage response, V, by Faraday's law becomes [8]

$$V = -N\frac{d\Phi}{dt} = -N\omega\Phi_0 \sin(\omega t), \tag{2}$$

which therefore, increases proportionally with the excitation frequency ω. In the proximity of the sample the induced eddy currents in the conducting aluminum also act to oppose the applied time-dependent flux, with the same frequency dependence as the excitation voltage. Therefore, the overall voltage response in the presence of the sample also increases proportionately with frequency in accordance with (2). Within the sample induced currents oppose the applied field, reducing the flux in the system. The resulting current densities within the conducting material may be related to this secondary voltage, V_S, which is induced within the sample, about a single closed current loop by [10],

$$V_S = \frac{1}{\sigma}\oint \mathbf{J}\cdot d\mathbf{l}, \tag{3}$$

where $\mathbf{J}$ is the current density in the sample, σ is the conductivity and the integral is about the closed current loop arising in the conducting plane. In the presence of a crack, the perturbation in the receive coil response will reproduce this linear dependence on frequency, resulting in greater current densities and an enhanced signal-to-noise response with increasing frequency according to (2) and (3). However, this is not the only consideration when evaluating the signal response. Skin depth, δ, is also a factor, since with increasing frequency the induced current densities are also concentrated closer to the surface according to the dependence given by [8]:

$$\delta = \sqrt{\frac{\rho}{\mu\omega}} \tag{4}$$

Table 2 Skin depths at various frequencies from (1) compared with a_{50}

Freq. kHz	Skin depth (mm)	Intimate contact probe a_{50} (mm)	Non-contact probe a_{50} (mm)
200	0.26	–	–
400	0.18	–	–
800	0.13	0.26	0.31
1600	0.09	0.15	0.18

where ρ is the resistivity, μ the permeability and $\omega = 2\pi f$, where f is the operating frequency of the eddy current instrument. Table 2 shows the calculated skin depths at the four frequencies along with the determined a_{50} values at 800 and 1600 kHz for the contact and non-contact probes.

The relative decrease in current density J with respect to the surface density J_0 as well as the associated change in phase with depth z for a planar applied magnetic field is given by [8]:

$$J_{z/J_0} = e^{-z/\delta}\sin\left(\omega t - \frac{z}{\delta}\right), \tag{5}$$

where z is the depth into the conducting material. For smaller skin depths, depth of penetration is not as great since the attenuation is more rapid, but for the same sensing depth, z, the change in phase given by the ratio z/δ phase is greater. Therefore, the smaller skin depths at higher frequencies enhance the relative phase of the signal response with depth. This results in a phase angle that increases with frequency, as observed in Fig. 5, further improving the signal-to-noise ratio. Increased phase rotation at higher frequencies and the comparison of skin depth with a_{50} values in Table 2 supports the explanation that enhanced detectability of corner cracks at higher frequencies may be attributed to a greater relative voltage response and reduced depth of penetration, which generates a larger field perturbation as the eddy currents are forced to pass around the crack [8]. In practice, the limit to the benefits of increasing the frequency comes when the skin depth is approximately the same size as surface features such as pits or scratches.

Lift-off is also a factor, with proportional increases in the effect of lift-off with increasing frequency [8]. This acts against the enhanced signal-to-noise at higher frequencies but is ameliorated by the contact probe condition as demonstrated by the lower a_{50} and $a_{90/95}$ compared with that of the non-contact probe in Tables 1 and 2.

C-Scan display provides the human operator with an additional detection capability: that of pattern recognition. The human eye does an excellent job of pattern recognition and effectively integrates the information from many lines. The Lissajou figure represents only a single line in the C-scan

image. Integrating information from many lines would be expected to improve the detectability of cracks. In addition, the pattern allows the operator with a tool to discriminate against features that might give rise to a false positive, since their pattern in the C-scan may not have the characteristic shape of the signal from a crack. When the pattern recognition of the C-scan is combined with strip-chart and impedance plane displays more reliable identification of cracks is obtained. In addition, identification of superposition of multiple crack sites and specific location of cracks may also be identified, all of which further aids the characterization of cracks within the bolt hole. Finally, this data may be recorded and stored for future analysis and comparison with subsequent examinations. These features are not as readily available with a simple impedance plane display, which nominally allows the identification and recording of a single maximum amplitude signal. Available C-Scan acquisition software however, also permits the examination of the Lissajou at points within the C-Scan permitting the identification of a maximum amplitude signal.

As mentioned earlier, the $a_{90/95}$ value of 0.22 mm for the proximity probe was made without any false calls. In part, this illustrates the robustness of using C-scan to identify cracks as discussed above; however, it is also a function of the way the tests were conducted. The specimens were cycled until at least one clear crack indication was present. This tended to produce a conservative approach to claiming a hit, since if one was unsure about the presence of a crack, one could cycle the specimen for another period and then check again. The crack would not have grown much during this period, but its signature pattern could have become much more defined. Hence there was a tendency to wait until one was certain. This is equivalent to setting a high threshold. This is a different situation from inspecting a series of specimens as is commonly done. In that situation, one cannot obtain confirmation by waiting. With the technique used in this paper, once one crack was identified, it is possible that a second or third crack might also be identified in the C-scan and this might be a false call. This would be a more unbiased call since the decision to stop the test had already been taken. However, no such false calls occurred. If there was an excessive tendency to conservatism this would only push the value of $a_{90/95}$ higher.

One might possibly expect the way in which the testing was done would introduce a bias to a lower value of $a_{90/95}$ for the steel non-contact probe. When the samples were examined using this probe, the decision that there was at least one crack had already been made using the more sensitive proximity probe. Hence, the operator could be biased to calling a hit. However, an examination of the hit/miss data in Figs. 9 and 10, shows that some points that were labelled hits in the former are labelled as misses in the latter. This suggests that the examiners were largely able to keep this bias out of their analysis. This is reflected in the substantially higher $a_{90/95}$ for the non-contact probe. A similar bias could have occurred for the lower frequencies, especially because C-scan images from all four frequencies could be lined up across the computer screen. However, if anything these tended to show the superiority of working at the higher operating frequency, as defects that were very pronounced at 1600 kHz were invisible in the C-scans at the lower two frequencies.

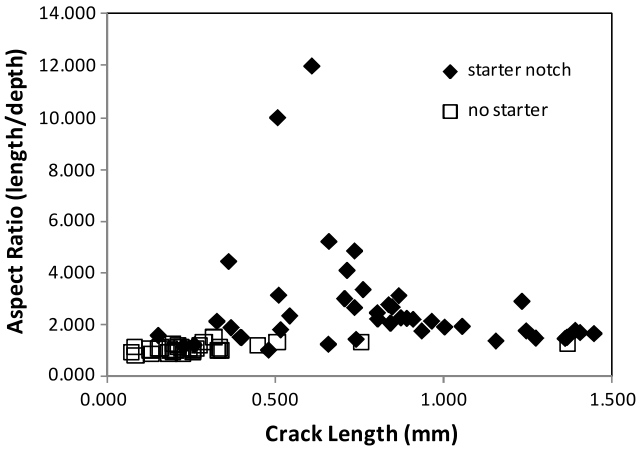

Fig. 12 Aspect ratio as a function of crack length for two data sets, one using a starter notch [5] and one where no starter notch was used [11]

The use of starter notches can readily result in cracks with very unrealistic aspect ratios. Figure 12 shows the aspect ratio of corner cracks generated using a starter notch [2], while those produced here did not. The data obtained from cracks not produced with a starter notch is very consistent with a mean aspect ratio of 1:1. In the case of the former, there is substantially more scatter, making it particularly difficult to consistently generate cracks at the detection threshold.

5 Summary

A number of parameters that may enhance detection of cracks in bolt hole eddy current have been examined. It has been clearly shown that the POD obtained from fatigue cracks in Al 7075 T6 using an eddy current bolt hole scanner can be optimized by operating the system at higher excitation frequencies. In the current study the POD obtained by operating at 1600 kHz was half as big as that obtained using an excitation frequency of 800 kHz and substantially better than that which would be obtained at 400 kHz. The higher frequency improves the sensitivity of the detector and localizes the eddy currents closer to the surface of the bolthole, increasing signals from small cracks. The phase angle of crack signals at higher frequencies is also greater, resulting in a greater separation of the signal from lift-off, which further enhances detectability. However, higher frequencies

also amplify the signal from surface defects and lift-off. This places a practical lower bound on the size of the crack that can be detected. This is projected to be when cracks have similar dimensions to surface features in the hole.

Using C-scan has several advantages over conventional bolt hole eddy current because the signal from small cracks has a characteristic shape in the C-scan, which can be used to help identify them and help prevent false calls. Operating at 1600 kHz, the value of $a_{90/95}$ using C-scan was found to be 0.22 mm using a proximity probe or 0.33 mm using a non-contact probe.

Acknowledgements The authors would like to thank Mike Bunn at the Aeronautical Engineering Research Squadron (ATESS), Trenton for technical assistance. The authors would also like to thank Dr. Abbas Fahr and Muzibur Khan from the National Research Council of Canada for allowing access to data from the Generic Bolt Hole Eddy Current Project. This work was supported by the Aerospace Research Advisory Committee (AERAC) and Academic Research Program (ARP) at the Royal Military College of Canada.

References

1. Berens, A.: NDE reliability data analysis. In: Nondestructive Evaluation and Quality Control. ASM International Metals Handbook, 9th edn., vol. 17, pp. 689–701
2. Khan, M., Yanishevsky, M., Fahr, A.: Bolt hole eddy current testing probability of detection, Part—I: Experimental design and data analysis. In: 12 International Conference on Fracture', Ottawa, 13–17 July (2009)
3. Department of Defense Handbook: Nondestructive Evaluation System Reliability Assessment, MIL-HDBK 1823 (2007 Update), Feb 2007
4. Charles Annis, P.E.: (2008) Statistical best-practices for building Probability of Detection (POD) models. R package mh1823, version 2.5.4, http://StatisticalEngineering.com/mh1823/
5. Lemire, H., Underhill, P.R., Krause, T.W., Bunn, M., Butcher, D.J.: Improving probability of detection of bolt hole eddy current inspection. Res. Nondestruct. Eval., **21**(3), 141–156 (2010)
6. Lemire, H., Krause, T.W., Bunn, M., Butcher, D.J.: Variables affecting probability of detection in bolt hole eddy current inspection. In: Thompson, D.O., Chimenti, D.E. (eds.) Review of Progress in Quantitative Nondestructive Evaluation. vol. 28B, pp. 1808–1815. Melville, New York (2009). ISBN 978-0-7354-0629-2
7. Lemire, H.: Improving probability of detection for bolt hole eddy current inspection. M.Sc. Thesis, Royal Military College of Canada, February 2008
8. Cecco, V.S., Van Drunen, G., Sharp, F.L.: Eddy Current Manual. In: Test Method. Chalk River Nuclear Laboratories, AECL-7523, November 1981, vol. 1 (1981), p. 9, 13, 46 and 89
9. Pampel, F.C.: Logistic Regression: A Primer. Sage, Thousand (2000)
10. Griffiths, D.J.: Introduction to Electrodynamics, 3rd edn. Prentice-Hall, Upper Saddle River (1999), p. 306
11. Underhill, P.R., Krause, T.W.: Measurement of uncertainty in eddy current bolt hole crack measurements for use in POD. In: QNDE Conference, Kingston, Rhode Island, AIP Conference Proceedings, vol. 1211, pp. 1934–1940 (2010)